

Design and cyclic testing of a gusset plate connection for precast concrete buckling-restrained braced frames

Hannah D. Kessler, Kaitlynn M. Conway, Laura M. Redmond, and Garrett J. Pataky

- A test specimen was designed and constructed to represent a scaled partial model of a precast concrete buckling-restrained braced frame. A gusset plate connection was designed using the uniform force method (UFM).
- The specimen was tested under representative seismic loads.
- Study objectives were to test a partial system under representative seismic loads and to determine the applicability of the force distribution assumed by UFM.

Buckling-restrained braced frames (BRBFs) have become a well-established lateral-force-resisting system for steel construction. Buckling-restrained braces implemented in steel structures have been shown to possess enough rigidity to satisfy structural drift limits, provide significant energy absorption, and reduce forces on foundations and adjacent members.¹⁻⁴ Testing procedures for buckling-restrained brace subassemblages and design procedures for steel structures using buckling-restrained braces have been codified in the American Institute of Steel Construction's *Seismic Provisions for Steel Buildings* (AISC 341) since the 2005 edition.^{5,6} In contrast, there is an insufficient amount of laboratory experiments from which a codified method of design for BRBFs for precast concrete systems can be developed and, before the study described in this paper, no U.S. laboratory experiments had been conducted on the seismic performance of these systems.

Presently, the most common types of lateral-force-resisting system for precast concrete structures are shear walls and moment frames.⁷ Because both shear walls and moment frames can include cast-in-place elements, post-tensioned connections, and grouted connections, some of the inherent benefits of selecting a precast concrete system—such as quick erection time, improved quality control, and lower project costs—are limited.⁸

Buckling-restrained braces were recently used as the lateral-force-resisting system for a precast concrete structure in the New Madrid seismic zone of the United States.⁹ The

braces were selected because they eliminated the need for moment connections and shear walls and provided sufficient load capacity and seismic drift levels. Prior to approval, local building authorities required that the project team justify the use of this novel system. If the use of precast concrete BRBFs could be codified, it could reduce erection times and project costs for precast concrete construction in seismic zones.

Precast concrete BRBFs have only been examined via laboratory experiments by Guerrero et al.¹⁰ Although the BRBFs showed promising seismic performance, the detailing of the system reflected the standards used in Mexico and the results may not directly translate to structures in the United States. Numerical studies conducted by Oh et al.¹¹ indicated excellent seismic performance of a precast concrete frame system with steel buckling-restrained braces but did not explicitly account for joint failure modes.

The study presented in this paper aimed to fill a knowledge gap by experimentally evaluating a proposed connection from a buckling-restrained brace to a precast concrete beam and column. Design options for buckling-restrained brace connections and their impact on precast concrete beam and column designs were first examined. Given concerns about high gravity loads being transferred from the beam into the gusset plate, several statically determinate connection types that prevented gravity load transfer were first examined.¹² However, even the most promising of these options, a lug connection that connected only to the corbel, would have required unconventional design procedures. Ultimately for these reasons, a gusset plate connection designed by the uniform force method (UFM) was selected for physical testing.

The objective of this study was to determine the applicability of the force distribution assumed by the UFM to precast concrete BRBFs via a cyclic test on a gusset plate connection designed by UFM. Using a test approach adapted from buckling-restrained brace-to-steel frame connection tests executed by Coy,¹³ investigators used two servo-controlled hydraulic actuators to simulate the behavior of a partial precast concrete BRBF under load due to a seismic event.

Literature review

The design of gusset-type connections to precast concrete systems is of interest to researchers because recent experimental and numerical research has indicated promising performance of precast concrete BRBF systems. Guerrero et al.¹⁰ compared the performance of a one-third-scale precast concrete BRBF and a precast concrete frame of the same scale constructed without BRBFs and found that damage in the beams, columns, and joints was reduced in the BRBF specimen. However, as noted previously, this study was performed in Mexico and the detailing was different from that specified in U.S. concrete design standards. Numerical research by Oh et al.¹¹ demonstrated that a precast concrete frame system with buckling-restrained braces evaluated by the Federal Emergency Management Agency's *Quantification of Building*

Seismic Performance Factors (FEMA P695)¹⁴ methodology could be given a response modification factor of 8 for seismic design. This model did not explicitly capture damage within the joints, but the system behavior of the model was validated against the experimental results of Guerrero et al.¹⁰ Given the promising experimental and numerical results for system-level performance of precast concrete BRBF systems, investigation of the behavior of connections from steel BRBFs to precast concrete frame systems is warranted.

The most common design procedure for steel gusset plate connections is the UFM, which was developed by Thornton¹⁵ in conjunction with a joint American Society of Civil Engineers (ASCE) and AISC task group and first appeared in the *AISC Manual of Steel Construction*¹⁶ in 1992. The UFM was created to satisfy static equilibrium and assigns dimensions of the gusset's connected edges such that no moments occur on any of the three connection interfaces (gusset-to-beam, gusset-to-column, and beam-to-column). Because the load path through the gusset plate depends on the stiffness of the connections and the members that they attach, the analysis is indeterminate. This indeterminacy was neglected in the derivation of the UFM in the interest of creating an easily usable design method for distribution of interface forces due to brace action.

When Thornton derived the UFM,¹⁵ he acknowledged that distortion (referred to as frame action in this paper) causes additional positive and negative forces on the gusset due to the opening and closing of the angle between the beam and the column; however, the UFM recommends that frame action be ignored for concentric connections. In the AISC manual,¹⁶ this recommendation was justified by the agreement between the UFM's predictions and the experimental forces from idealized experimental tests by Gross and Cheok¹⁷ and Bjorhovde and Chakrabarti¹⁸ (described later). **Figure 1** shows variable and interface force locations for the UFM.

In the UFM, the following equations are used.

To assign the dimensions of the gusset connected edges based on the beam, column, and brace geometry, the following equation was used:

$$\alpha = \tan \theta (\beta + e_b) - e_c$$

where

α = distance from the face of the column to the centroid of the gusset-to-column connection

θ = angle between the centroid of the column and the centroid of the brace

β = distance from the face of the beam to the centroid of the gusset-to-column connection

e_b = one-half the depth of the beam

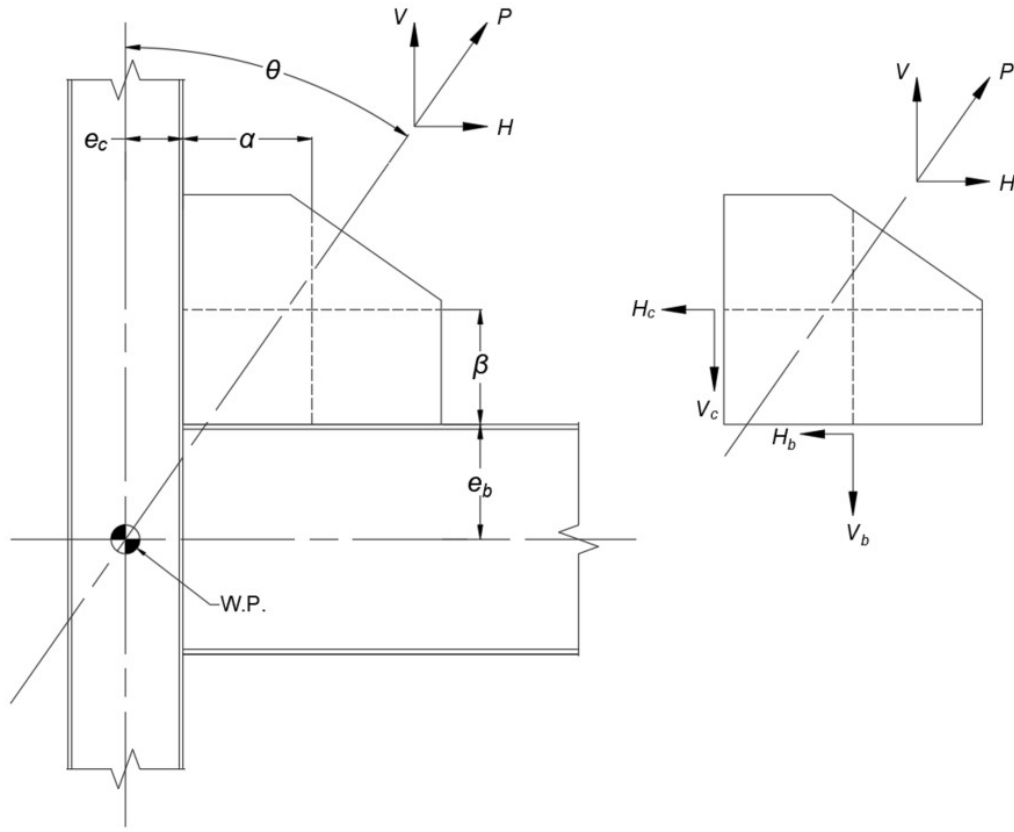


Figure 1. Variable definitions and location of gusset plate interface forces for the uniform force method. Note: e_b = one-half the depth of the beam; e_c = one-half the depth of the column; H_b = required shear force on the gusset-to-beam connection; H_c = required axial force on the gusset-to-column connection; V_b = required axial force on the gusset-to-beam connection; V_c = required shear force on the gusset-to-column connection; W.P. = work point; α = distance from the face of the column to the centroid of the gusset-to-column connection; β = distance from the face of the beam to the centroid of the gusset-to-column connection; θ = angle between the centroid of the column and the centroid of the brace.

e_c = one-half the depth of the column

To derive the distance between the work point and the centroid of the gusset plate, the following equation was used:

$$r = \sqrt{(\alpha + e_c)^2 + (\beta + e_b)^2}$$

where

r = distance between the work point and the gusset centroid

To distribute the brace load to the beam and column connected interfaces as shear and axial forces, the following equations were used:

$$H_b = \frac{\alpha}{r} P$$

where

H_b = required shear force on the gusset-to-beam connection

P = required brace axial force

$$V_b = \frac{e_b}{r} P$$

where

V_b = required axial force on the gusset-to-beam connection

$$H_c = \frac{e_c}{r} P$$

where

H_c = required axial force on the gusset-to-column connection

$$V_c = \frac{\beta}{r} P$$

where

V_c = required shear force on the gusset-to-column connection

The UFM was validated based on two different sets of idealized steel gusset connection tests. The first set of tests, completed by Gross and Cheok,¹⁷ were executed on subassemblages consisting of a stub of a continuous column between two floors, two stub braces, and one stub beam subjected to lateral loading. These stub members were all pinned at their midspans, the theoretical points of zero internal moment, during the tests. The gusset was connected to the beam using a fillet weld and to the column using clip angles. The clip angle was extended along to the beam web to create a pinned connection between the beam and the column. Although effort was made to simulate full-frame behavior, the boundary conditions of these tests were highly idealized. The UFM conservatively predicted a lower capacity than the actual tested capacities for all of the experiments by Gross and Cheok, with an average difference of 5%.

The second set of tests, completed by Bjorhovde and Chakrabarti,¹⁸ were executed on subassemblages consisting of a stub continuous column between two floors, one stub brace, and one stub beam loaded in tension at the free end of the stub brace. The stub column was pinned at both ends, and the ends of the stub beam and brace were left to rotate and translate freely. As in the tests by Gross and Cheok, the gusset was connected to the beam using a fillet weld and to the column using clip angles. This clip angle was extended to create the same type of pinned beam-to-column connection. Although effort was made to simulate full-frame behavior, the boundary conditions of these tests were highly idealized. The UFM conservatively predicted a lower capacity than the actual tested capacities for all of the experiments by Bjorhovde and Chakrabarti, with an average difference of 52%.

As stated, Thornton proposed that frame action can be ignored for concentric connections in his initial derivation of the UFM;¹⁵ however, more recent studies investigating the UFM's application to full steel frames with fixed connections^{19–22} have shown that frame action can alter the gusset interface forces significantly. Chou et al.¹⁹ concluded that the forces developed by frame action and brace action are similar at low frame displacements; however, at high frame displacements, the forces developed by frame action exceed those developed by brace action. Chou et al. also proposed an equation to predict the normal and shear forces developed by frame action based on the geometry of the connection, the stiffness of the gusset plate, the stiffness of the beam, and the stiffness of the column. Lin et al.^{20,21} concluded that forces due to frame action cause the experimental interface force distribution to deviate significantly from the UFM's predictions. Lin and colleagues found that the forces due to frame action were additive to the interface shear forces and subtractive to the interface normal forces. Cui et al.²² concluded similarly that gusset connection design should account for both brace action (force distribution predicted by the UFM or a similar model) and frame action.

Similarly, limited research has been conducted on braced frames consisting of cast-in-place concrete members and steel

buckling-restrained braces. Maheri and Yazdani²³ created finite element models tuned to the benchmark experimental tests of Maheri and Hadjipour²⁴ on cast-in-place concrete joints with steel gusset connections. The stub beam and column ends were allowed to freely translate and rotate, the beam-to-column joint was pinned, and pure tension was applied along the stub brace's longitudinal axis. Once sufficient agreement between the experimental results and initial finite element models was achieved, Maheri and Yazdani undertook a parametric study that varied the gusset geometry and brace angle. They concluded that the UFM could be applied conservatively for the design of steel brace connections to reinforced concrete structures. This work was highly idealized, much like the tests of Gross and Cheok¹⁷ and Bjorhovde and Chakrabarti.¹⁸ Tsai et al.²⁵ investigated the applicability of the UFM to gusset plates, attaching buckling-restrained braces to fixed cast-in-place concrete full frames. They concluded that the generalized UFM, a more general version of the UFM proposed by Muir,²⁶ was acceptable for prediction of force distribution at gussets in foundation-column-brace connections because frame action is minimized by the rigid foundation. Tsai et al. did not find generalized UFM alone to be acceptable for beam-column-brace connections.

Experimental test program

The work initiated in the study described in this paper aims to determine whether a steel gusset plate connection designed by the UFM would be sufficient for seismic design of a precast concrete system with buckling-restrained braces. Although the shortcomings of the UFM have been noted in the studies with fixed connections, it remains the most common method for sizing and design of steel gusset plates and distributing the brace force to the connected components. In addition, precast concrete systems are much closer to a pinned condition than the fixed frames investigated by Tsai et al.²⁵ For these reasons, the UFM was selected as the design method for the gusset plate in this first experimental test on this system.

Prototype structure and design loads

A four-story parking structure (three elevated levels) was selected as the prototype structure for the experiment. BRBFs were a replacement for the shear walls typically used as the lateral-force-resisting system in parking structures. Two bays of BRBFs per story were required to replace one shear wall. The story height was 9 ft 11 $\frac{1}{2}$ in. (3.045 m), and the bay width was 16 ft 0 in. (4.877 m). These dimensions represent the average story height and average bay width derived from three example parking structure projects provided by a local precast concrete producer. The resulting angle between the brace and the beam was approximately 32 degrees. **Figure 2** illustrates the full-scale prototype bay.

The test specimen was scaled to one-third for area, 0.577 for length, and one-third for force. This ensured equivalent stresses between the test and prototype structures. The maximum 90 kip (400 kN) brace force in the test structure corresponded

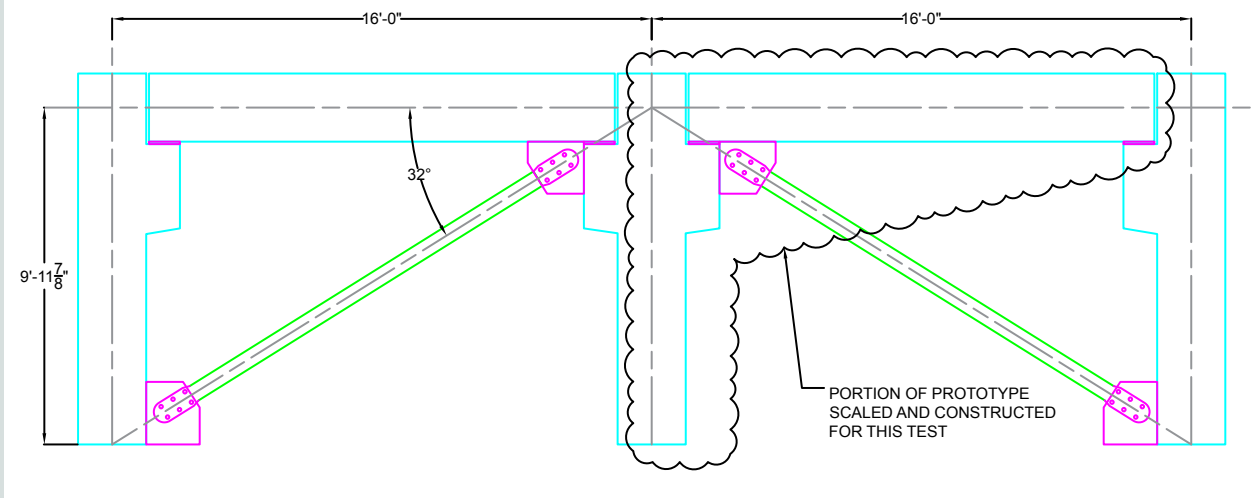


Figure 2. Full-scale prototype bay diagram, including partial frame constructed for the test program. Note: 1" = 1 in. = 25.4 mm; 1' = 1 ft = 0.305 m.

to a 270 kip (1200 kN) brace force in the full-scale prototype. This 270 kip load was greater than the required brace loads of all floors of a six-story seismic design category B example parking structure and all five stories of a seismic design category C example parking structure.

The buckling-restrained brace manufacturer, CoreBrace, used a frame model designed using structural analysis software to determine a full-scale prototype brace size and overstrength factors that would induce a maximum adjusted brace strength of 270 kip (1200 kN) in compression at the elongation caused by 2% story drift, $\Delta h_{2\%}$. The maximum adjusted brace strength, overstrength factors, and frame displacements were scaled appropriately for design of the test specimen. All test specimen brace connections and members adjoining the brace were designed to resist this maximum adjusted brace strength per AISC 341-16 section F4.²⁷ Gravity and live loads were determined in accordance with ASCE 7-16, *Minimum Design Loads and Associated Criteria for Buildings and Other Structures*.²⁸

Test specimen design and construction

Because the test frame was designed as pinned, a partial frame could be tested in lieu of the whole frame. The members of the partial frame were scaled but were of complete scaled length; this design meant that a realistic pinned column base connection could be tested and realistic beam and column curvature could be monitored. The prototype precast concrete specimen in context of the full frame is shown within the dashed outline in Fig. 2.

The gusset plate dimensions were sized using the test loads (neglecting gravity loads) and the UFM as it is outlined in chapter 13 of the 15th edition of the AISC *Steel Construction Manual*.²⁹ The randomly oriented fiber bearing pad at the

beam-to-column bearing and a difference between the prescribed and as-built conditions caused a 3/4 in. (19 mm) gap between the bottom of the beam and the top of the embedded plate at the corbel. This gap was accounted for by assigning load to the beam and column using the full length of the gusset (assuming no gap) at the beam and column interfaces but applying the column vertical and horizontal force components at the center of the connected interface (accounting for the gap) at the column. To maintain equilibrium, a small moment was developed at the column interface. The design of the gusset plate and its connections accounted for this moment, which is described by the following equation and shown in Fig. 3.

$$M_c = V_c e_c + V_b \left(e_c + \frac{l_b}{2} \right) - H_b e_b - H_c \left(e_b + l_g + \frac{l_c - l_g}{2} \right)$$

where

M_c = required moment on the gusset-to-column interface

l_b = length of gusset interface connected to beam

l_g = length of gap between bottom of beam and top of corbel

l_c = length of gusset interface connected to column

All relevant gusset, bolt, and weld failure modes were checked in accordance with the corresponding sections J2 and J3 of ANSI/AISC 360-16, *Specification for Structural Steel Buildings*³⁰ using directions from AISC's *Design Guide 29: Vertical Bracing Connections—Analysis and Design*.³¹ Although 3/16 in. (4.8 mm) fillet welds using 80 ksi (552 MPa) electrodes were specified along the gusset's connected edges, 3/8 in. (9.5 mm) fillet welds using 70 ksi (483 MPa) electrodes were fabricated. This difference in the as-built condition

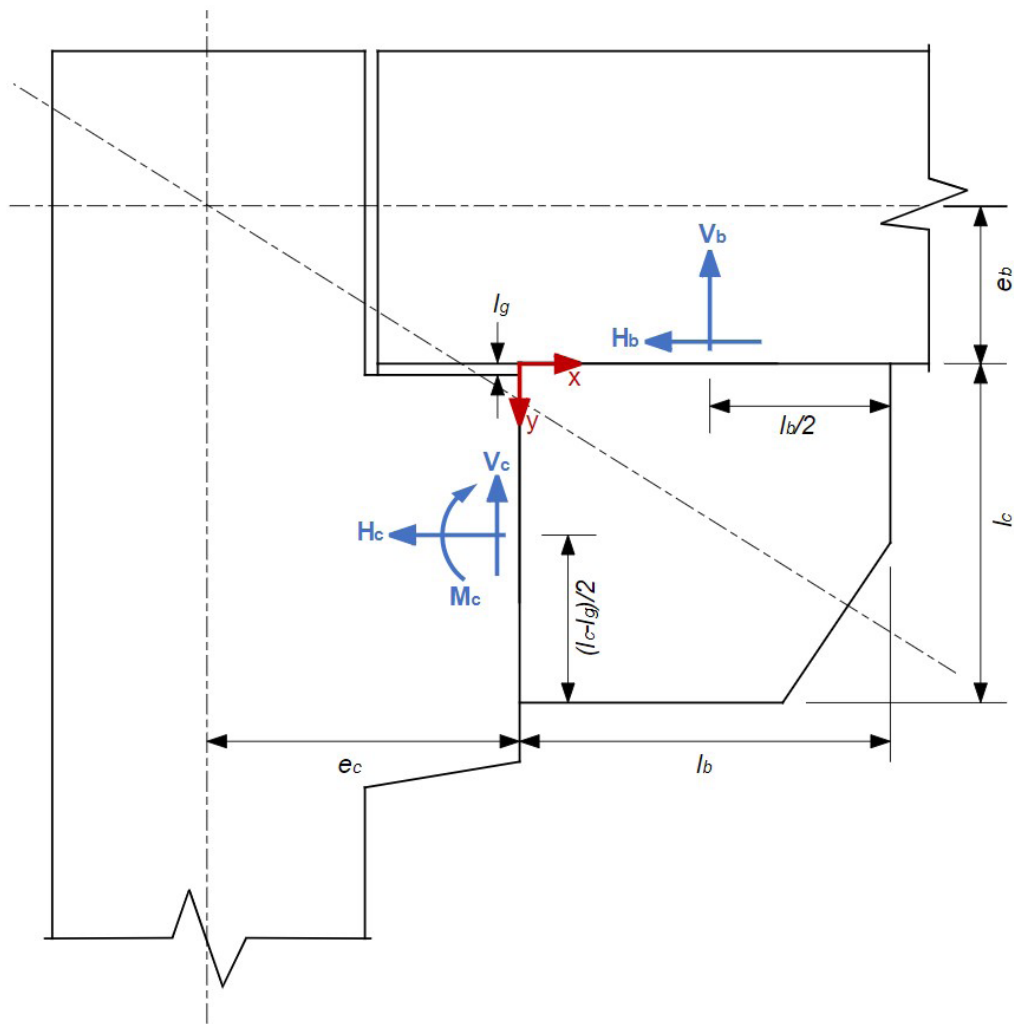


Figure 3. Interface force distribution adjusted for gap between the beam and corbel. Note: e_b = one-half the depth of the beam; e_c = one-half the depth of the column; H_b = required shear force on the gusset-to-beam connection; H_c = required axial force on the gusset-to-column connection; l_b = length of gusset interface connected to beam; l_c = length of gusset interface connected to column; l_g = length of gap between bottom of beam and top of corbel; M_c = required moment on the gusset-to-column interface; V_b = required axial force on the gusset-to-beam connection; V_c = required shear force on the gusset-to-column connection.

added additional conservatism to the design. Yield of embedded plates at the beam and column were checked using finite element models.¹² Bars welded to embedded plates were designed to resist combined shear and tensile forces in accordance with chapter 22 of the American Concrete Institute's *Building Code Requirements for Structural Concrete (ACI 318-19) and Commentary (ACI 318R-19)*.³²

The jumper plate connection was modified from a typical precast concrete beam-to-column connection provided by a local precast concrete producer. Typical connections use headed studs that do not transfer uplift. Because the connection for the test specimen was required to transfer uplift at this location, deformed bar anchors with headed terminators were necessary. Shear and flexure of the jumper plates were checked in accordance with ANSI/AISC 360-16 sections

F11 and G4.³⁰ Although $\frac{7}{8}$ in. (22.2 mm) fillet welds using 80 ksi (552 MPa) electrodes were specified along the jumper plate edges, fillet welds with a $\frac{5}{16}$ in. (7.9 mm) root that used 110 ksi (758 MPa) electrodes had to be fabricated due to warping of the embedded plates. The strength of the as-built condition was sufficient when rechecked in accordance with ANSI/AISC 360-16 section J2. The reinforcing bars welded to the embedded plates of the jumper connection were designed in the same manner as those incorporated into the gusset plate connection. **Figure 4** shows the jumper plate and gusset plate connections.

Although this test frame should have, in theory, been pinned—meaning it should not have been required to transmit large moments—the beam and column were detailed to resist moment because it provided the most ductility and conserva-

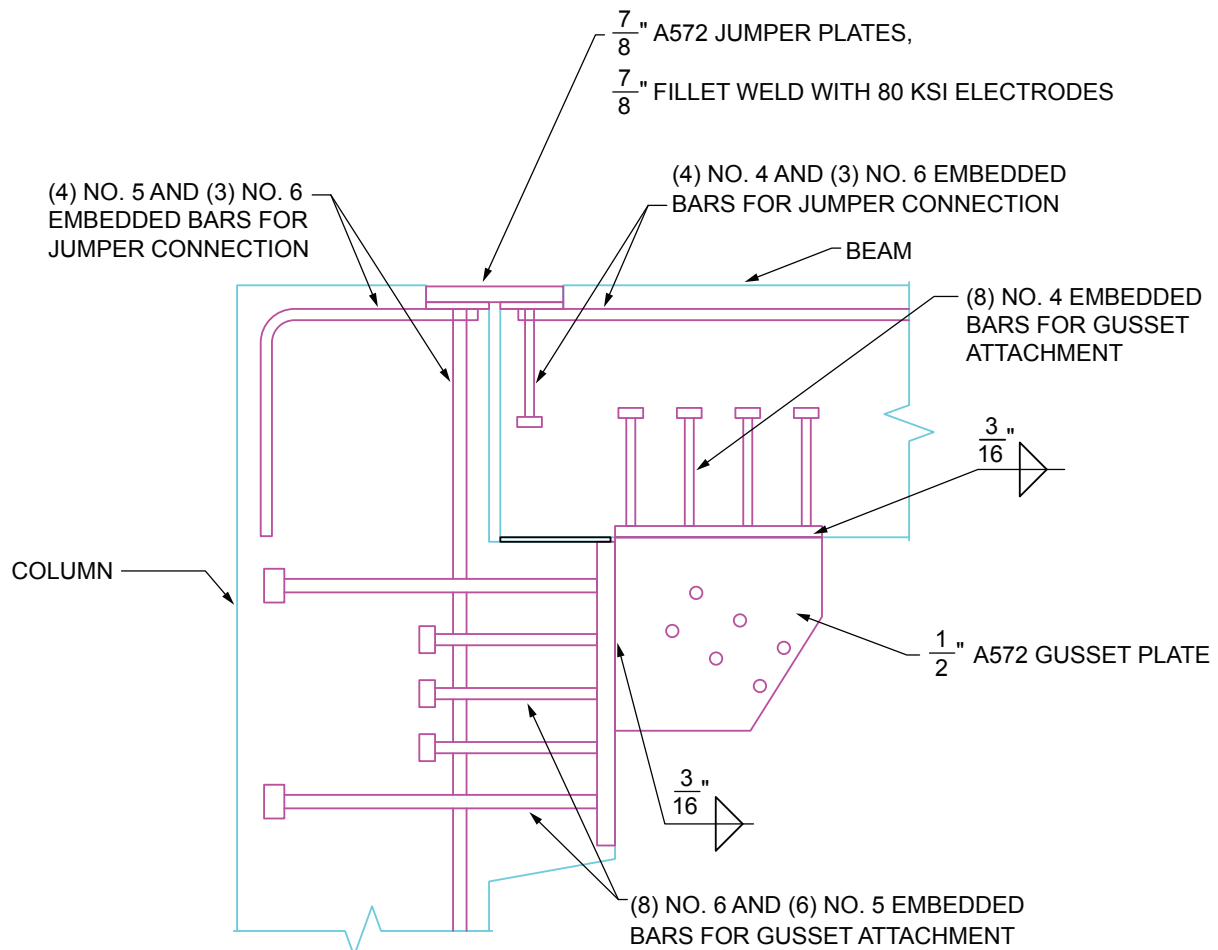


Figure 4. Jumper plate and gusset plate connections. Note: no. 4 = 13M; no. 5 = 16M; no. 6 = 19M; 1" = 1 in. = 25.4 mm; 1 ksi = 6.895 MPa.

tism for this precast concrete BRBF design. The beam was designed to meet the requirements of ACI 318-19³² section 18.6, “Beams of Special Moment Frames,” and detailed in accordance with ACI 318-19 chapter 25. The column was designed to meet the requirements of ACI 318-19 section 18.7, “Columns of Special Moment Frames,” and detailed in accordance with ACI 318-19 chapter 25. The resulting scaled beam design used Grade 60 (414 MPa) reinforcing bars and 6000 psi (41 MPa) concrete. The full beam reinforcing schedule is shown in **Fig. 5**, and the full column reinforcing schedule is shown in **Fig. 6**.

The corbel was designed to meet the requirements of ACI 318-19³² section 16.5, “Brackets and Corbels,” and detailed in accordance with ACI 318-19 chapter 25. The factored normal load on the corbel was greater than the factored shear load, in violation of the requirement in ACI 318-19 section 16.5.1.1 for the use of the cantilever beam method of corbel design. The section 16.5.1.1 requirement is stipulated because the cantilever beam method has only been validated for cases

where factored normal load is less than factored shear load. The cantilever beam method (ACI 318-19 section 16.5) was selected for this frame because it is more commonly used than the strut-and-tie method (ACI 318-19 chapter 23) and because it can provide a potential data point on the performance of corbels designed by the cantilever beam method for cases where the factored normal load is less than the factored shear load. The resulting scaled corbel design used Grade 60 (414 MPa) reinforcing bars and 6000 psi (41 MPa) concrete. The corbel reinforcing schedule is shown in **Fig. 6**.

A widely used pinned precast concrete column base connection was chosen for this frame. This connection consisted of a base plate that was embedded in the column base using reinforcing bars welded to the plate. The base plate was flush with the outside dimensions of the column, so the four anchor bolts were inset in pockets at the plate corners. The base plate was designed according to section 6.11 of the eighth edition of the *PCI Design Handbook*.⁷ The lapped splices between the reinforcing bars welded to the base plate and the longitudinal bars

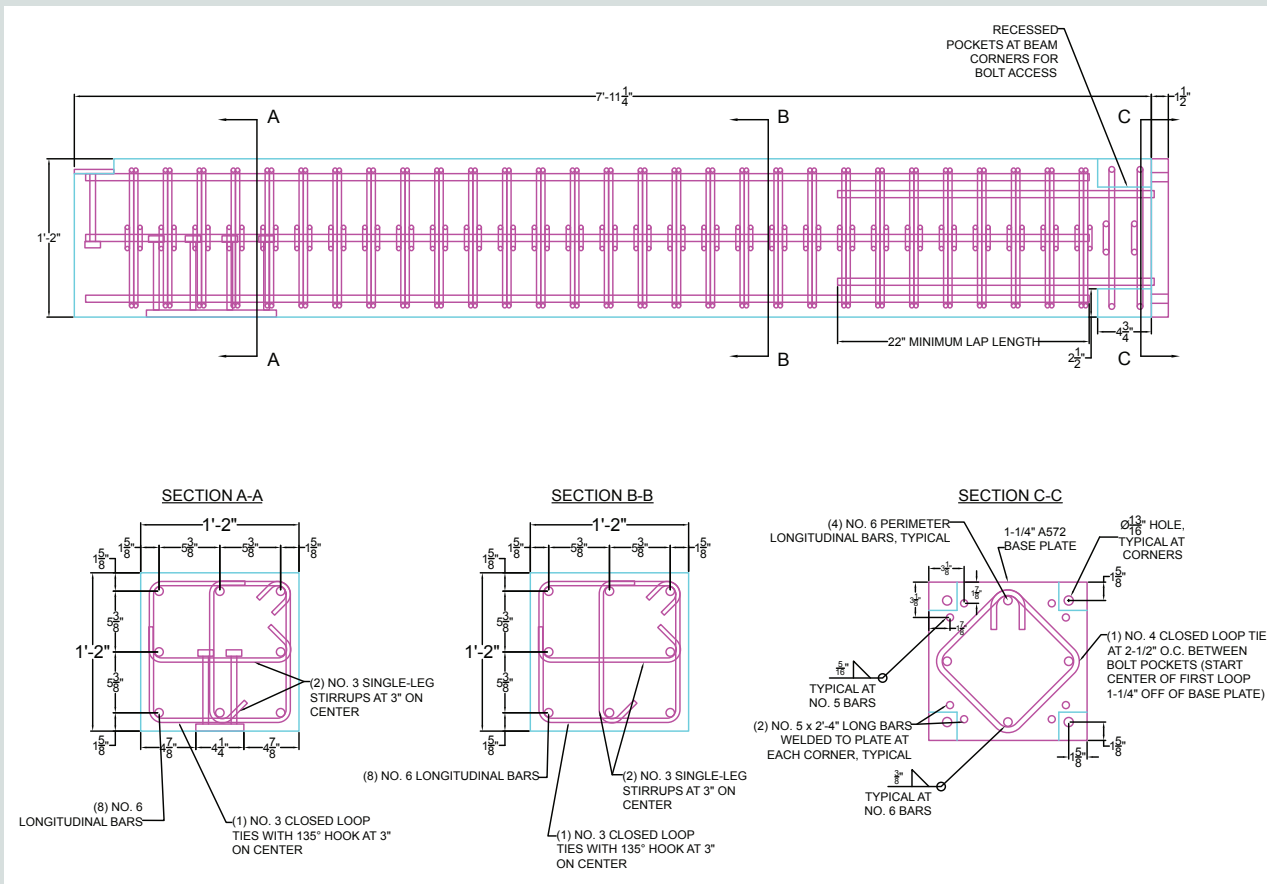


Figure 5. Beam reinforcing schedule. Note: no. 3 = 10M; no. 4 = 13M; no. 5 = 16M; no. 6 = 19M; 1" = 1 in. = 25.4 mm; 1' = 1 ft = 0.305 m.

that were terminated above the bolt pockets were designed to meet the requirements of ACI 318-19 section 25.5.2.³² The base plate used ASTM A572³³ Grade 50 (345 MPa) steel and was 1.25 in. (31.8 mm) thick, the reinforcing bars were Grade 60 (414 MPa), and 1.25 in. diameter Grade A490 bolts were used. The same connection was used to attach the beam to its actuator. These connections can be viewed in section C-C of Fig. 5 and section C-C of Fig. 6.

Typically, bolt pockets would be grouted solid after the column is installed and the bolts or threaded rods have been tightened sufficiently; however, in this study, the column base was designed to provide sufficient shear capacity without grouting the bolt pockets so that the test specimen could be easily removed from the frame.

Several challenges were encountered during the design process. First, it was difficult to find space to place the large amounts of reinforcing that were required both physically and by the special moment frame detailing requirements inside the beam and column. Second, there were several tolerance issues due to warping of the steel embedded plates prior to testing. Warping occurred at the jumper embedded plates and at the column base plate. The modification of the jumper plate welded connection to adjust for warping was discussed

previously. The warping of the base plate at the column caused the two bolts farthest from the strong floor to not be in contact with the reaction frame. Washers were added between the base plate and reaction frame at these locations for better contact.

Reaction frame and loading protocol

A reaction frame with a typical section size of HP18x135 was used for testing this specimen horizontally on the floor of the testing facility (Fig. 7–8). Three out-of-plane restraints—a corner brace against the precast concrete specimen itself, a brace on the beam actuator, and a brace on the brace actuator—were provided to ensure that the specimen could not move more than 0.05 in. (1.3 mm) in the vertical direction during testing. These restraints were in contact with the component they were restraining, but the component could slide using plastic sheets with low coefficients of friction and grease. The precast concrete specimen itself was supported using greased steel rollers.

Gravity load was neglected on the beam and column in the experimental setup. It was assumed that the buckling-restrained braces and gusset plates would be installed in the prototype structure after the floor topping had been poured and cured,

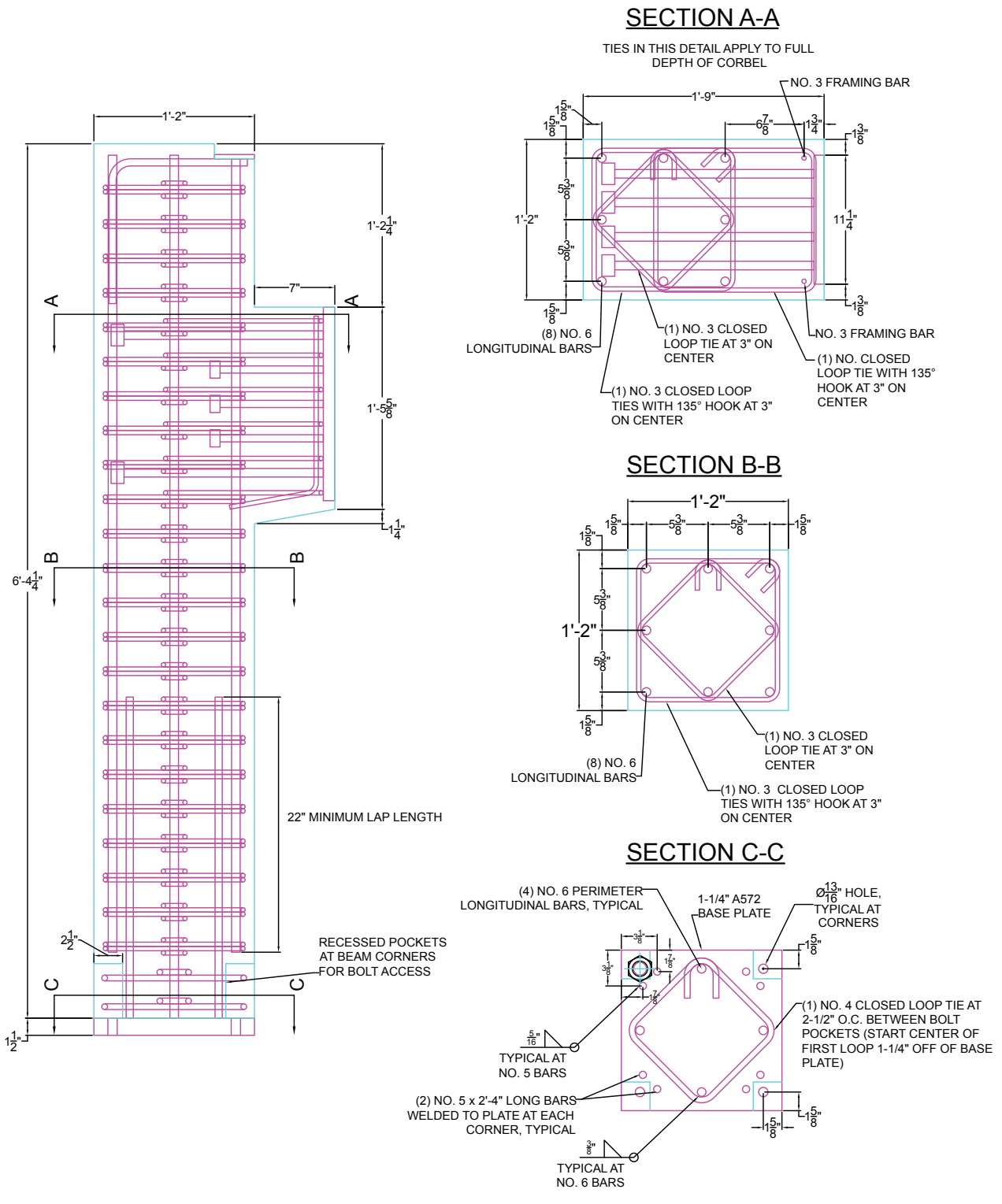


Figure 6. Column and corbel reinforcing schedules. Note: no. 3 = 10M; no. 4 = 13M; no. 5 = 16M; no. 6 = 19M; 1" = 1 in. = 25.4 mm; 1' = 1 ft = 0.305 m.

preventing as much gravity load transfer as possible. The gravity load that would pass through the corbel was 1.15 kip (5.12 kN), which was less than 6% of the UFM estimate of the highest vertical portion of the brace load to pass through

the corbel (20.8 kip [92.5 kN]). Although column gravity loads would have been present in the prototype structure, the primary focus of the experimental work was to characterize load path in the connection, which would be largely unaffec-

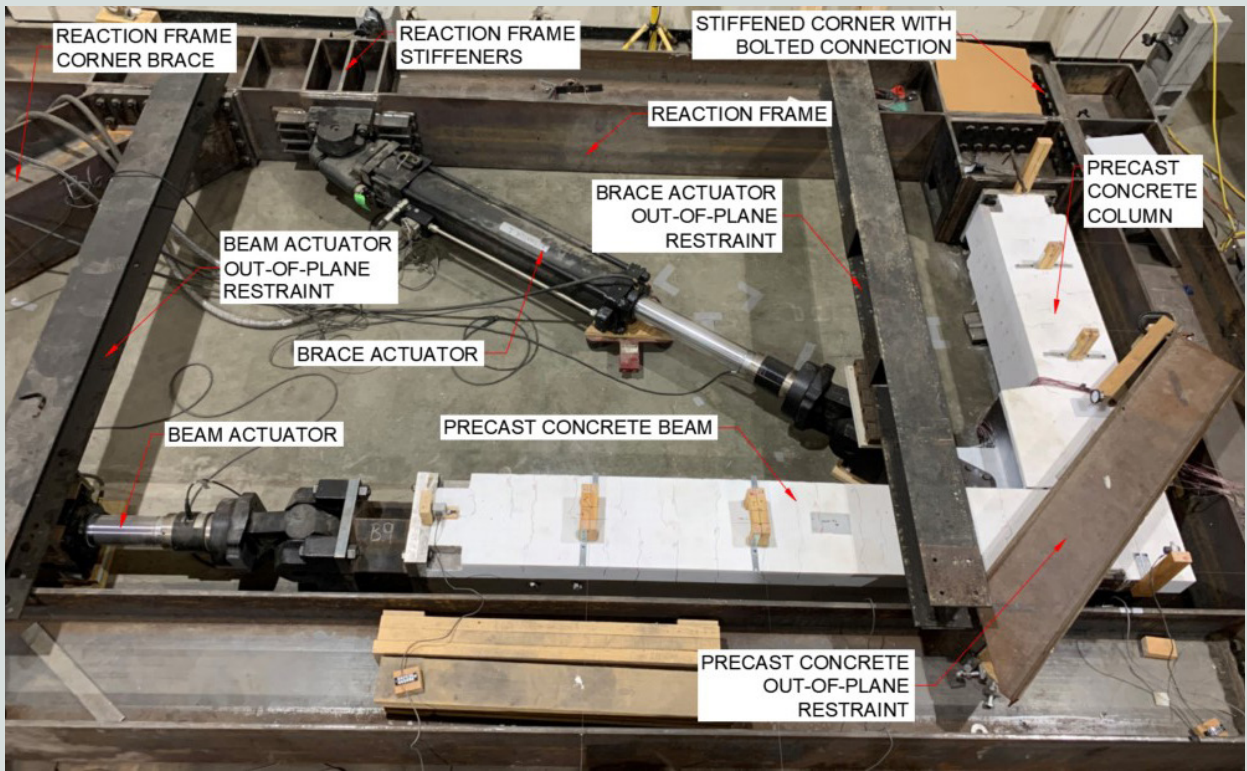


Figure 7. Precast concrete specimen (white) installed in the reaction frame.

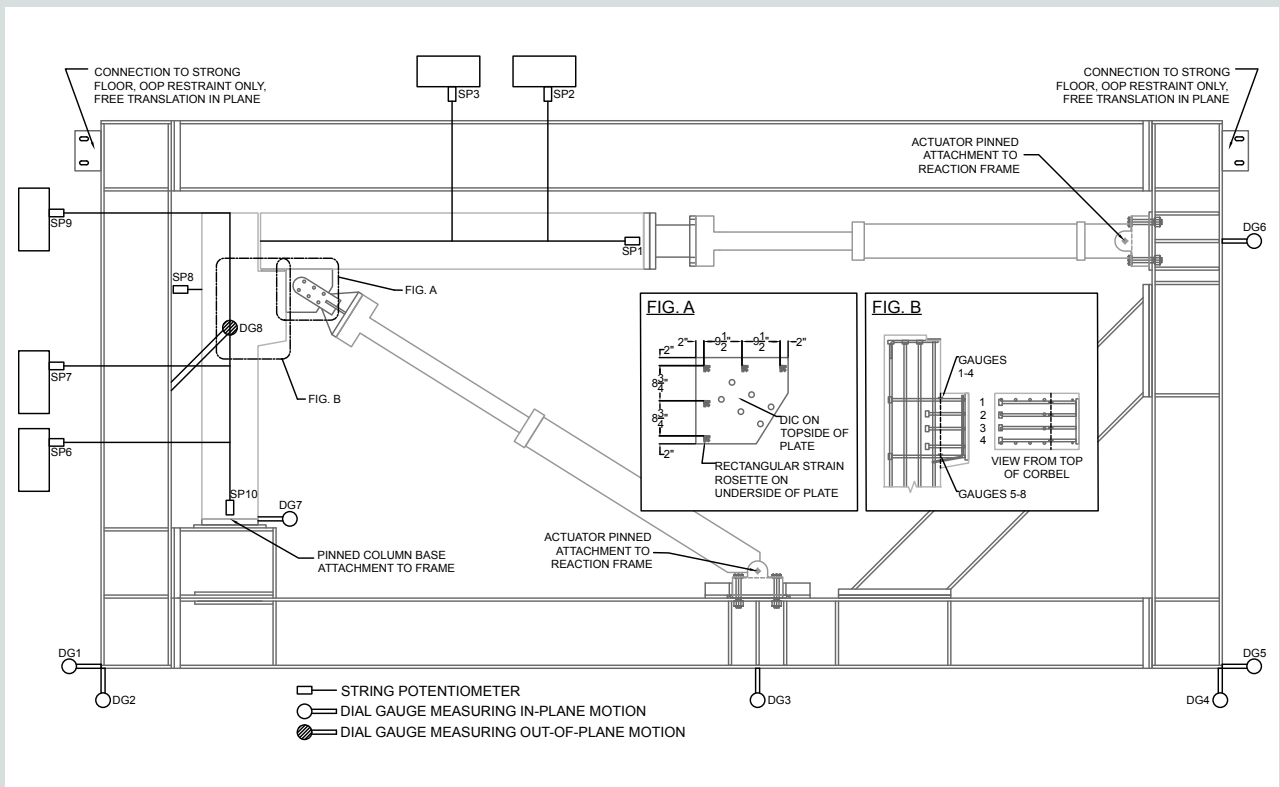


Figure 8. Instrumentation plan, including gusset plate instrumentation (Fig. A) and corbel reinforcing bar instrumentation (Fig. B). Note: DG = dial gauge; DIC = digital image correlation; OOP = out-of-plane; SP = string potentiometer. 1" = 1 in. = 25.4 mm.

ed by gravity load in the column. Only test loads were used to design the gusset plate connection.

The behavior of a buckling-restrained brace was simulated with a servo-controlled hydraulic actuator. The hysteresis of a representative buckling-restrained brace with a peak compression force of 270 kip (1200 kN) was generated using the backbone of hysteresis provided by CoreBrace and a re-created version of the hysteresis generation procedure proposed by Coy.¹³ This process involved the derivation of multiple stress-strain relationships (consisting of portions of linear and nonlinear behavior) for several strain levels. These stress-strain relationships were validated with existing experimental data and comparison between the experimental hysteresis and the hysteresis predicted using the derived stress-strain relationships yielded a satisfactory level of accuracy.¹²

The hysteresis was then scaled appropriately for the one-third-length scale specimen shown in white in Fig. 7. The full hysteresis was derived for the simulated brace at the following fractions of the strain, strain levels, in the brace at 2% story drift: 1/8, 1/4, 1/2, 3/4, and 1. In addition, this full hysteresis included strain levels corresponding to one-half yield strain and yield strain. Each strain level, hereafter referred to as *procedure*, of this full hysteresis was broken into multiple discrete steps for testing. Each procedure was planned to have two cycles, that is, each procedure was planned to be executed twice. The full

prescribed and unadjusted experimental hysteresis divided into the seven procedures executed are shown in Fig. 9.

Instrumentation

The instrumentation plan is shown in Fig. 8. Rectangular rosette strain gauges were applied along the connected edges to validate the force distribution predicted by the UFM. These rectangular rosette gauges allowed for the determination of normal and shear strains along the connected interfaces in a manner similar to that used in other gusset plate tests in the literature.^{17,18,22} The strain gauges were applied to the underside of the gusset plate (Fig. 8). Linear strain gauges were applied to each of the eight corbel bars at the critical section of the corbel (Fig. 8) because the corbel primary tension reinforcing bars were determined to be the weakest link if the assumed UFM load distribution was correct. The gauges on the corbel bars were applied at the theoretical point of highest stress.

Both of the servo-controlled hydraulic actuators were equipped with integrated load cells and linear variable displacement transducers (LVDTs). These allowed for monitoring of internal force and displacement in the precast concrete beam and the simulated brace. Curvature of the beam and column were monitored using string potentiometers and dial gauges. String potentiometers 1 and 10 were placed along

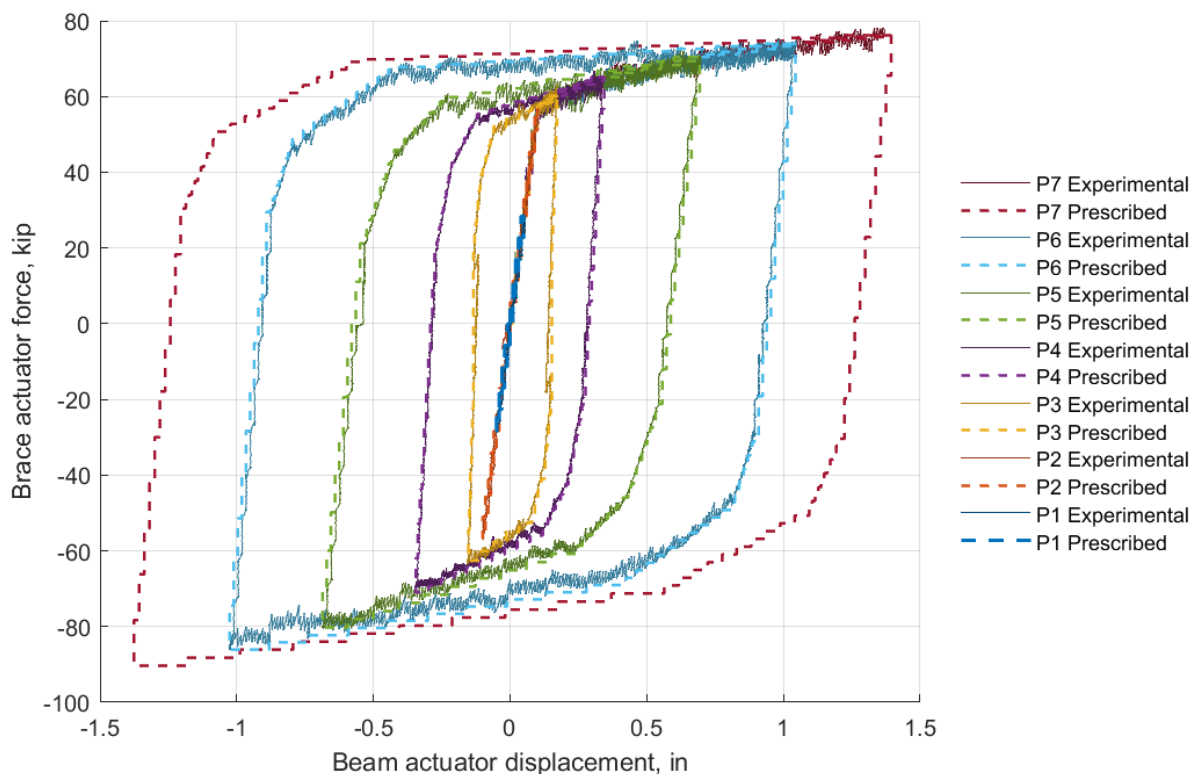


Figure 9. Prescribed and experimental hysteresis for procedures 1 through 7 (P1-P7). Note: 1 in. = 25.4 mm; 1 kip = 4.448 kN.

the longitudinal axes of the beam and column and monitored axial deformation (Fig. 8). String potentiometers 6 through 9 were placed perpendicular to the column longitudinal axis at quarter points along the column height to measure curvature. String potentiometers 2 and 3 were placed perpendicular to the beam longitudinal axis at the first two quarter points along the beam length to measure curvature.

One dial gauge was placed at the column base to monitor the slip of the column base. Another dial gauge was placed at the five-eighths point of the column (measured from its base) to monitor the out-of-plane movement of the precast concrete specimen. The in-plane movement of the reaction frame was also monitored through use of dial gauges. These gauges were placed at the free corners of the reaction frame and at the actuator-to-frame attachment points.

Digital image correlation was used along with the physical strain gauges to provide a complementary set of measurements. Digital image correlation was used to measure the deformations on the top of the plate in the areas not covered by the lug connector. A two-camera setup in a stereo system was used to capture the full three-dimensional (3-D) deformation of the plate to understand bending and out-of-plane deformation of the plate occurring during loading. The plate was painted white and stamped black with a random speckle pattern. Images were captured with Flir Grasshopper3 digital cameras and Schneider Kreuznach Xenoplan 1.9/35 lenses. The stereo setup was 70 in. (1778 mm) above the specimen, with the cameras spaced 16 in. (406 mm) apart. Strain calculations were performed in Vic 3D from Correlated Solutions Inc., with Gaussian weights, a step size of 5 pixels, a strain window of 5 subsets, and a subset of 55 pixels to create a virtual strain gauge of 21 pixels and a spatial resolution of 75 pixels. The maximum sigma, a measure of uncertainty in the digital image correlation procedure, was 0.075 mil (0.002 mm).

Test procedure

The servo-controlled hydraulic actuator that simulated the buckling-restrained brace is referred to as the brace actuator. The second actuator, referred to as the beam actuator, induced frame horizontal displacement. A fraction of the maximum displacement of a given procedure was applied with the beam actuator first, and then the brace actuator was adjusted to the corresponding brace force of each procedure. These steps were repeated until two stair-stepped versions of each of the seven procedures had been completed (Fig. 9). The specimen was brought back to its zero displacement and force position at the end of each cycle of each procedure.

The test data collected were a mixture of continuous and discrete measurements. Continuous measurements were taken at a rate of 1 Hz for all strain gauges and string potentiometers 6 through 10. Continuous digital image correlation measurements were taken at a rate of 1 Hz (procedures 1, 3, 5, and 6) and 0.25 Hz (procedure 4); digital image

correlation measurements were not taken for procedure 7. Manual measurements for string potentiometers 1, 2, and 3 and all dial gauges were taken at points where the procedure changed slope. The precast concrete beam and column were whitewashed to improve the visibility of cracks that formed during testing. After each cycle was completed, the accessible sides of the beam and column were visually inspected with the aid of a flashlight. The length and width of any cracks found during this inspection were measured. After the cracks were measured, the cracks were traced with marker and the procedure and cycle number were written next to the crack.

After all measurements were taken and cracks were inspected for a given cycle, the next cycle was completed in the same fashion. This process continued until two cycles of each procedure had been completed consecutively for procedures 1 through 6. Procedure 7 was terminated early because the beam actuator capacity was reached.

Results and discussion

Frame force versus displacement behavior

Figure 10 shows a comparison of the prescribed hysteresis and the load and frame displacement at the cycle peaks adjusted to account for slip at the column base. The slip was accounted for by subtracting the slip at each peak from the prescribed displacement at each peak. Note that procedure 7 could not be completed in full because the beam actuator hit the safety limit of 98 kip (436 kN) on its tension capacity.

The column base bolt holes were 0.125 in (3.175 mm) oversized, so some slip occurred at the column base. Because continuous measurements could not be taken at the column base during the test, it was not possible to actively compensate for the slip. Thus, only procedures 5, 6, and 7, which had the least error due to slip, were used for the posttest analysis. The maximum slips as a percentage of the beam LVDT readings in tension were 13% for procedure 5, 10% for procedure 6, and 9% for procedure 7. In addition, the entire hysteresis could not be adjusted for the column base slip because slip measurements were taken only at the peaks with a mechanical dial gauge. For this reason, Fig. 10 shows the prescribed hysteresis and the peak points adjusted for the maximum slip observed at the column base at these peak hold points.

The displacements at the beam were also calculated from interpolations of the column curvature from the string potentiometer readings for procedures 4, 5, 6, and 7. The displacements measured during procedures 1, 2, and 3 were close to or below the minimum increment that could be measured by the string potentiometers and could not be reliably used for calculating slip compensation during the test. The displacements interpolated from the string potentiometer readings had an average 12% error (compared with the beam actuator LVDT measurements for cycles 5, 6, and 7) and a maximum

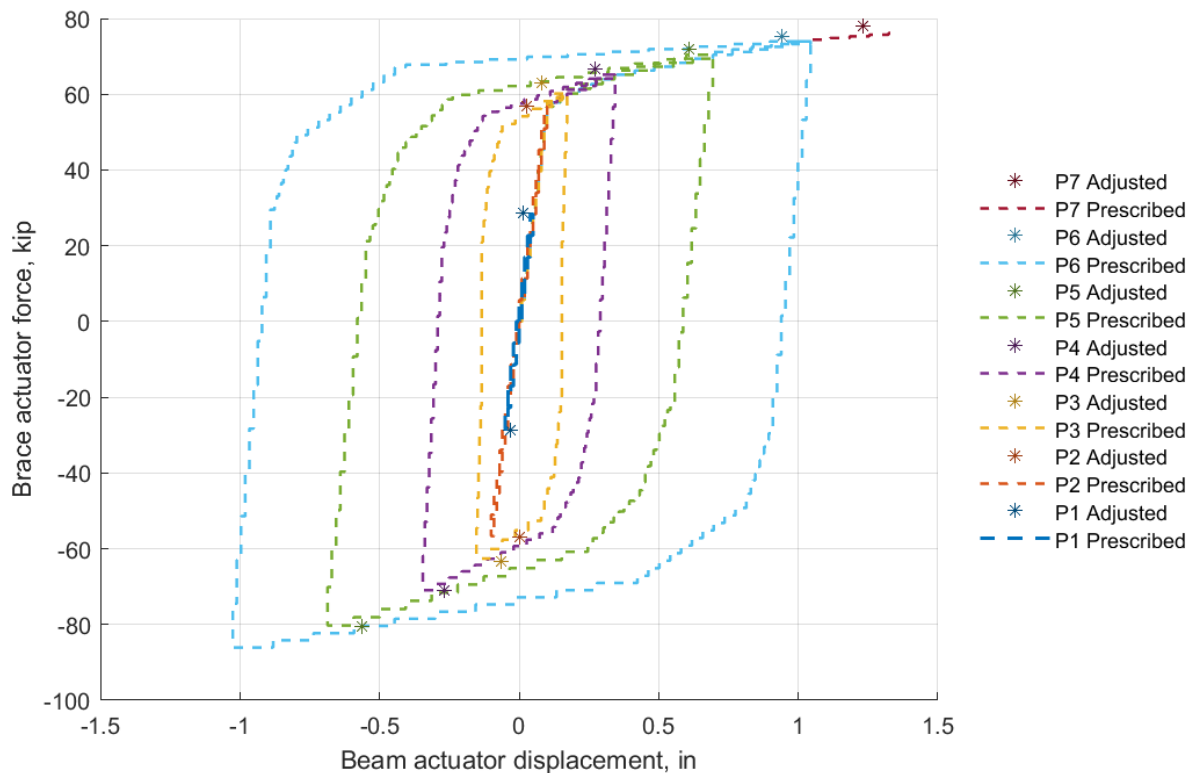


Figure 10. Prescribed hysteresis compared with the load and adjusted frame displacement at the cycle peaks during procedures 1 through 7 (P1-P7). Note: 1 in. = 25.4 mm; 1 kip = 4.448 kN.

of 15% error. Because procedures 5, 6, and 7 were the most relevant cycles, they were used to examine the gusset plate strains and force distributions.

Out-of-plane motion

Data from the string potentiometers and dial gauges helped quantify the incidental out-of-plane motion and were compared with the out-of-plane motion detected by the digital image correlation at the gusset plate. The maximum out-of-plane motions in compression recorded by dial gauge 8 (DG8) on the column and by digital image correlation on the gusset plate were 0.011 and 0.031 in. (0.279 and 0.787 mm), respectively. The maximum out-of-plane motions in tension recorded by DG8 on the column and by digital image correlation on the gusset plate were both 0.022 in. (0.559 mm).

Forces in the beam actuator

Although the precast concrete BRBF was assumed to be fully pinned for design purposes, the experimental results did not match this assumption. The difference between the measured beam force and the theoretical (fully pinned) force increased as the magnitude of prescribed brace force increased (**Fig. 11**). This deviation begins to be particularly significant in procedure 5 (maximum brace load of 70.4 kip [313 kN]), with a frame displacement corresponding to $0.5\Delta h_{2\%}$. Except

for procedure 7, two cycles of each procedure were executed and achieved behavior near the desired hysteresis unadjusted for slip (**Fig. 9**). Because the distribution of force between the members did not follow the pinned design assumption, the beam actuator hit the safety limit on its tension capacity (098 kip [436 kN]), which was just a bit lower than peak load and displacement in tension for procedure 7.

Gusset plate strains and interface forces

Virtual extensometers were added in the post-processed digital image correlation data at 16 locations along the beam interface and 16 locations along the column interface, for a total of 96 virtual extensometers. The virtual extensometers were placed approximately 1 in. (25.4 mm) from the beam or column face to allow for direct comparison with the values measured by the physical strain gauges. The virtual extensometers were 0.4 in. (10.2 mm) long and measured the engineering strain along the gauge. Because the strains measured on the gusset plate remained elastic throughout the duration of the test, the experimental stresses were determined along the gusset's connected edges using the elastic and shear moduli (E and G , respectively) of the plate and Hooke's law. Out-of-plane effects were neglected when calculating plate stresses because the magnitude of out-of-plane motion of the specimen was small in general and similar between the tension and compression cycles.

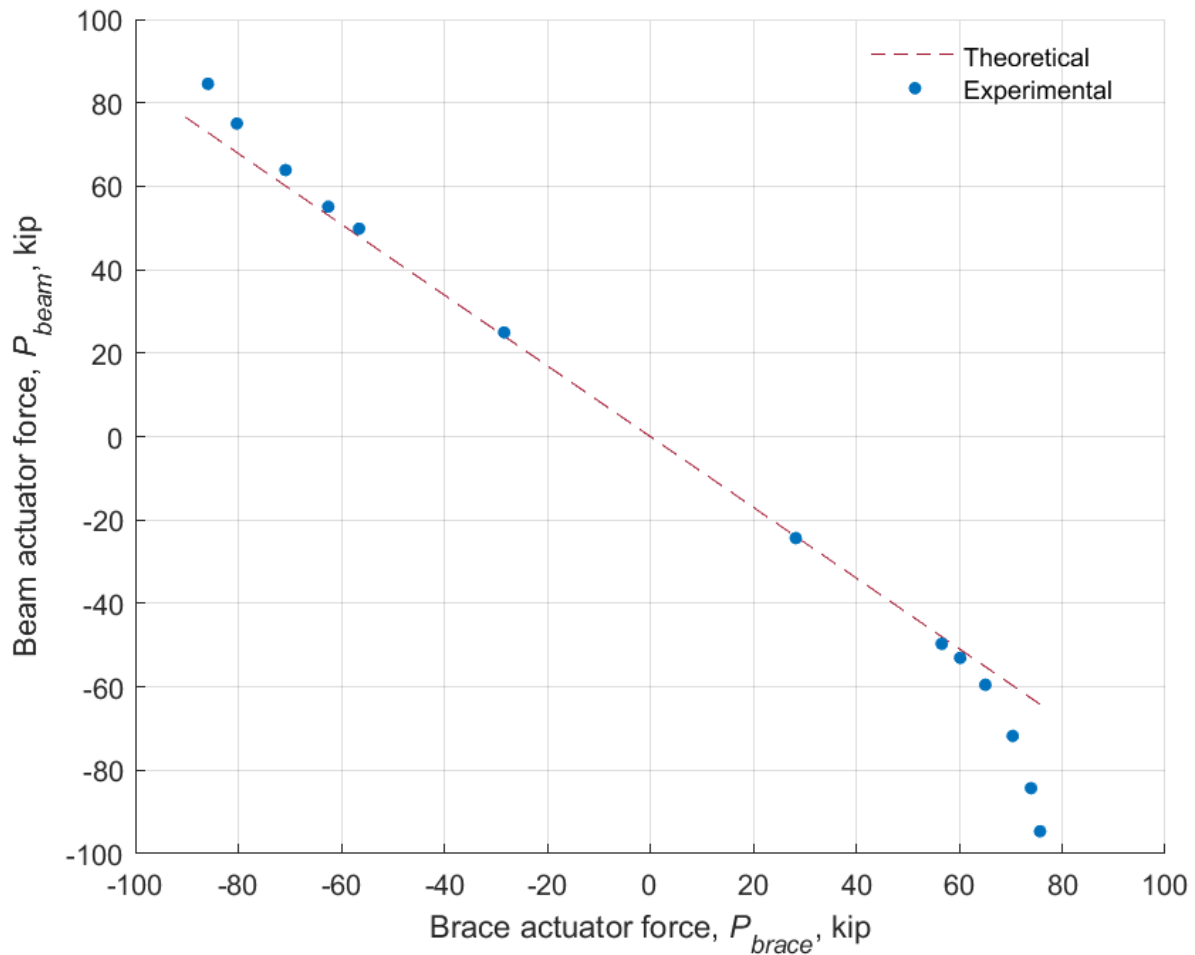


Figure 11. Brace internal force versus beam internal force, both theoretical (fully pinned) and experimental. Note: 1 kip = 4.448 kN.

The strains measured by digital image correlation for procedures 1 through 4 were near the noise floor of the digital image correlation system and not used in the posttest analysis. The strains measured by the digital image correlation for procedures 5 and 6 were sufficiently greater than the experimental noise level and were therefore more meaningful. In addition, procedures 5, 6, and 7 had significantly less influence from the slip at the base of the column. The five virtual extensometers along the beam interface that were closest to the free edge of the gusset plate were in an area of heavy shadow, which caused higher values of sigma, a measure uncertainty, in that region.³⁴ Results from these five virtual extensometers were discarded in the analysis. **Figure 12** shows the location of these five virtual extensometers and a map of sigma across the entire gusset plate for procedure 5 cycle 1, which are also representative of procedures 5 and 6.

As a second source of data for the gusset plate strains and interface forces, data from the strain gauges on the backside of the gusset plate were compared with the results of the digital image correlation. **Figure 13** shows the strain gauge and virtual extensometer normal and shear stresses along

the column connected interface for procedure 5 cycle 1. **Figure 14** shows the strain gauge and virtual extensometer normal and shear stresses along the beam connected interface for procedure 5 cycle 1.

Trends are included in Fig. 13 and 14. A linear trend was chosen for the normal stresses, and a second-order polynomial trend was selected for the shear stresses. The average root mean square deviations between the trends fit to the strain gauge data and the virtual extensometer data were 3.40 and 2.83, respectively, for the normal stress trends and the shear stress trends.

Contrary to what would be expected from the UFM, the experimental normal stress trends were not constant along the beam- and column-connected edges. This finding indicates that some moment developed along both the beam and column interfaces. The assumption that only the column-connected interface would see a moment because of the gap at the beam-corbel bearing is likely incorrect, as shown by the linear but not constant normal stress trends in Fig. 13 and 14. Although this gap likely contributes to the development of

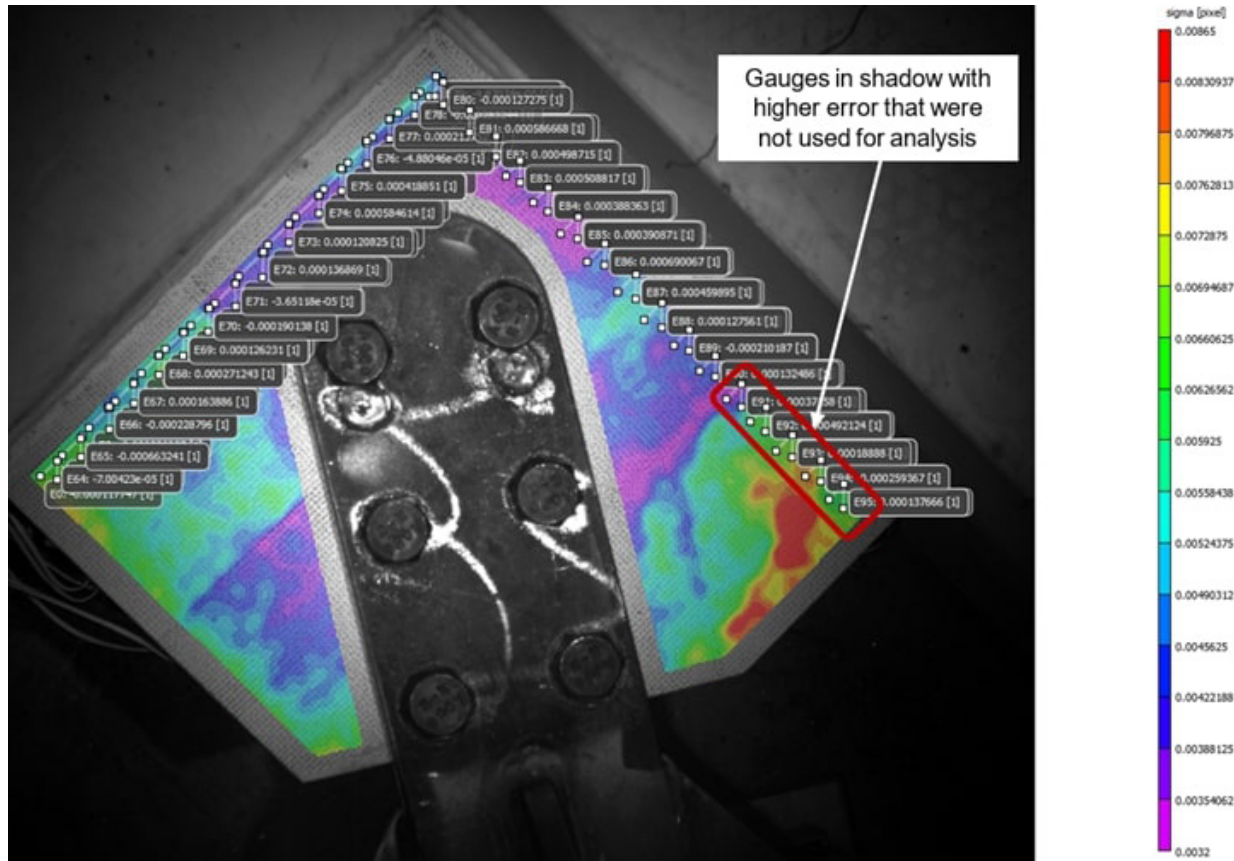


Figure 12. Map of sigma, a representation of uncertainty, across the gusset plate for procedure 5 cycle 1 and the location of the five virtual extensometers that were discarded for analysis.

moments along these interfaces, it cannot be isolated as the only cause.

Experimental interface forces for procedure 5 cycle 1 and procedure 6 cycle 1 were determined using the trends of the strain gauge and virtual extensometer data while the brace was in tension. The integral under each of these trends over the length of the connected edge was taken and multiplied by the thickness of the gusset plate to determine the experimental interface forces. This process is described in Eq. (1) through (4).

$$V_b = t_g \int_0^{l_b} \sigma_b(x) dx \quad (1)$$

where

t_g = thickness of the gusset plate

$\sigma_b(x)$ = experimental normal stress distribution along beam-connected interface

$$H_b = t_g \int_0^{l_b} \tau_b(x) dx \quad (2)$$

where

$\tau_b(x)$ = experimental normal stress distribution along beam connected interface

$$V_c = t_g \int_0^{l_c} \tau_c(y) dy \quad (3)$$

$$H_c = t_g \int_0^{l_c} \sigma_c(y) dy \quad (4)$$

where

$\sigma_c(y)$ = experimental normal stress distribution along column connected interface

The resulting experimental interface forces as determined from strain gauge and virtual extensometer data and their percentage differences for procedures 5 and 6 are presented in **Table 1**. There was less than 20% difference between the values determined for H_b and V_c and less than 100% difference for V_b and H_c . The experimental values of H_c , as calculated from the strain gauge data, were consistently positive and increased throughout the cycles, as would be expected, whereas the sign of these same values as calculated from the virtual extensometer data flipped sign between procedure 5 and procedure 6. Because of the agreement between the strain gauge and virtual extensometer trends and the expected signs

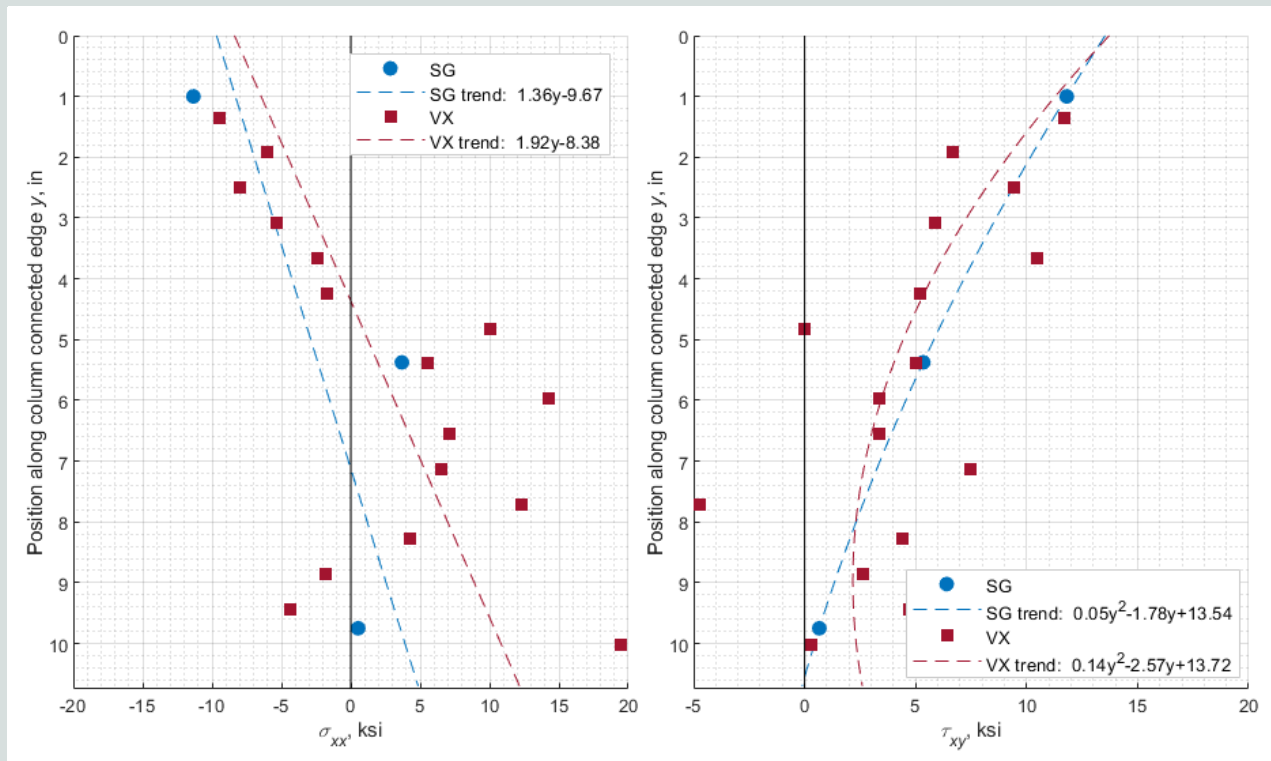


Figure 13. Stress along the column connected interface. Note: SG = strain gauge; VX = virtual extensometer; σ_{xx} = experimental normal stress on beam-connected interface; τ_{xy} = experimental shear stress on beam- and column-connected interfaces. 1 in. = 25.4 mm; 1 ksi = 6.895 MPa.

and increase of the strain gauge data, it was deemed acceptable to determine the experimental interface forces for all procedures using only this data set and the same process from Eq. (1) through (4).

Table 2 displays the theoretical interface forces (as derived from the UFM), experimental interface forces determined by integrating under the strain gauge trend, the percent error between the two, and the sign of this error for procedures 5, 6, and 7 at the brace's peak tension load. For procedures 5 and 6, the values from the procedure's first and second cycles were averaged. An average for procedure 7 was not necessary because only one cycle was completed. The error in procedures 1 through 4 was not included because it was established that the slip at the column base affected the results of these procedures more substantially.

The percent error between the theoretical predictions of the UFM and experimental values for all interface forces was generally high (>51%) in all procedures. Generally, the percent error increased in magnitude as the procedure number increased (that is, as a larger brace force was applied to the system). Through all cycles, the beam had higher forces along its longitudinal axis (shear) than the column (H_b versus V_c). The beam initially had larger normal interface forces than the column, but by the latter procedures, the column had larger normal forces than the beam (V_b versus H_c). The most important observation is that V_b and H_c , the normal interface

forces, generally had a negative percent error, and H_b and V_c , the shear interface forces, generally had a positive percent error. This finding suggests that, like similar fixed-frame tests from the literature^{21,22,25} where force due to frame action was subtractive to interface normal force and additive to interface shear force, this system was significantly affected by frame action, although its connections were not fully fixed.

The theoretical ratios of V_c/V_b and H_c/H_b were 0.77 and 2.43, respectively, for all procedures. The average experimental ratios (taken over procedures 5, 6, and 7) of V_c/V_b and H_c/H_b were 4.69 and -0.39, respectively. The minimum experimental ratio of V_c/V_b , 3.01, occurred in procedure 5 and the minimum experimental ratio of H_c/H_b , -0.48, occurred in procedure 7. The maximum experimental ratio of V_c/V_b , 7.29, occurred in procedure 6 and the maximum experimental ratio of H_c/H_b , -0.29, occurred in procedure 5. According to the UFM, V_c and V_b should act in the same direction and H_c and H_b should act in the same direction. In the experiment, negative ratios of H_c/H_b occurred when this was not the case. Generally, the magnitude of the ratios of V_c/V_b and H_c/H_b increased with increasing brace load and frame displacement; this finding implies that the column saw more load than the beam increasingly as the procedure number increased.

Strains in the reinforcement

Of the eight linear gauges attached to the corbel primary

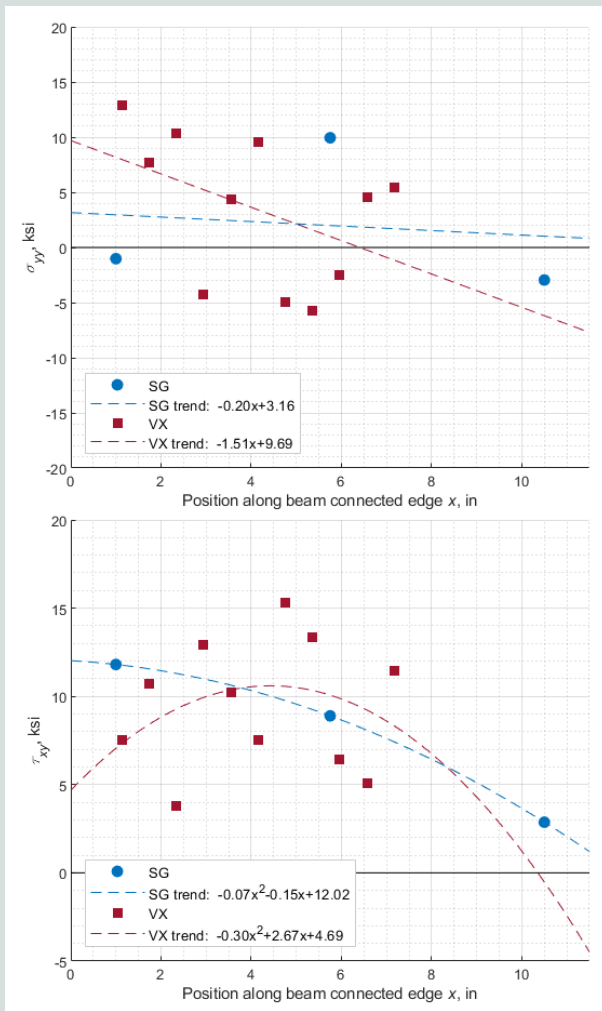


Figure 14. Stress along the beam connected interface. Note: SG = strain gauge; VX = virtual extensometer; σ_{yy} = experimental normal stress on column-connected interface; τ_{xy} = experimental shear stress on beam- and column-connected interfaces. 1 in. = 25.4 mm; 1 ksi = 6.895 MPa

reinforcing, two gauges on the top row of reinforcing and two gauges on the bottom row of reinforcing were responsive. All measured strains on the corbel reinforcing remained in the elastic range, with the largest strain recorded at any bar equal to 6% of yield strain (0.00207). Strains in the gauged corbel reinforcing bars were significantly lower than what was expected. There are two likely causes for these very low strain gauge readings:

- First, eight no. 6 (19M) corbel primary tension reinforcing bars and six no. 5 (16M) supplemental bars were provided to prevent undesirable plate bending at the corbel embedded plate. Although it was assumed only the eight no. 6 bars would carry interface force to the corbel in design, it is likely that the supplemental six no. 5 bars also carried some of the interface forces.
- Second, the strain gauges were adhered along the longitudinal axis of the bars, and the gauges would therefore

Table 1. Experimental interface forces as determined from strain gauge and virtual extensometer data and their percent difference for procedures 5 and 6

Procedure	Parameter	Interface force			
		V_b	H_b	V_c	H_c
5	SG trend, kip	-10.23	-46.61	-30.78	13.38
	VX trend, kip	-5.71	-38.80	-29.08	-10.42
	% difference	-57	-18	-6	n/a
6	SG trend, kip	-5.22	-62.84	-38.04	25.11
	VX trend, kip	-1.85	-69.43	-33.64	15.67
	% difference	-95	-10	-12	46

Note: H_b = required shear force on the gusset-to-beam connection; H_c = required axial force on the gusset-to-column connection; n/a = not applicable (this percent difference was not calculated due to the unexpected sign difference between the strain gauge and virtual extensometer data); SG = strain gauge; V_b = required axial force on the gusset-to-beam connection; V_c = required shear force on the gusset-to-column connection; VX = virtual extensometer. 1 kip = 4.448 kN.

only effectively measured tension or compression in this direction. As discussed previously, the corbel interface axial loads were generally lower than expected from the UFM force distribution, which would reduce bar longitudinal strains. Larger shear interface forces than predicted from the UFM were observed on the corbel, but these forces are primarily carried in the noninstrumented stirrups or through dowel action in the longitudinal bars, which would have been difficult to observe using the strain gauges as oriented in this test.

Variation of force distribution with increasing brace load

One possible cause of the increase in percent error between the theoretical and experimental beam force and the increase in magnitude of V_c/V_b and H_c/H_b ratios would be an increase in column base fixity with increasing brace load. A change in column fixity is a reasonable explanation, given the column connection was not an idealized true pin, but reflective of typical “pinned” precast concrete connections.

Another possibility is that the interface force distribution changed with the change in relative damage between the beam and column. However, the relative amount of cracking observed in the beam compared with the column did not follow a consistent trend through the procedures. The damage was initially similar, then occurred more on the beam, and finally approached more similar crack spacings and locations.¹²

Table 2. Theoretical interface forces, experimental interface forces, percent errors, and error signs for procedures 5, 6, and 7 at the brace's peak tension load

Procedure	Parameter	Interface force			
		V_b	H_b	V_c	H_c
5	Theoretical, kip	-21.16	-17.38	-16.24	-42.31
	Experimental, kip	-10.23	-46.61	-30.78	13.38
	% error	-51.6	168.2	89.5	-131.6
	Error sign	-	+	+	-
6	Theoretical, kip	-22.21	-18.25	-17.06	-44.42
	Experimental, kip	-5.22	-62.84	-38.04	25.11
	% error	-76.5	244.4	123.0	-156.5
	Error sign	-	+	+	-
7	Theoretical, kip	-22.74	-18.68	-17.46	-45.47
	Experimental, kip	-11.11	-68.21	-41.79	33.01
	% error	-51.1	265.2	139.4	-172.6
	Error sign	-	+	+	-

Note: The values from the first and second cycles for procedures 5 and 6 were averaged; values for procedure 7 are from the one cycle completed. H_b = required shear force on the gusset-to-beam connection; H_c = required axial force on the gusset-to-column connection; V_b = required axial force on the gusset-to-beam connection; V_c = required shear force on the gusset-to-column connection. 1 kip = 4.448 kN.

Conclusion

From the results presented, it is concluded that the partial precast concrete BRBF tested was not similar enough to the idealized pinned connections from Bjorhovde and Chakrabarti¹⁸ and Gross and Cheok¹⁷ that were used to verify the UFM to assume this force distribution. During the test, a positive percent error was observed between the theoretical UFM and experimental shear interface forces and a negative percent error between the theoretical UFM and experimental normal interface forces. These findings align with Lin's conclusions²¹ from tests on fixed frames that shear force induced by frame action is additive to interface brace force and normal force induced by frame action is subtractive. This research implies that frame action significantly affects the distribution of forces at the gusset interfaces, even though the tested frame has more flexibility than the fixed frames from the literature.^{20–22,25}

Despite the force distribution varying from the UFM assumed for design, the connection was robust enough to prevent failure. At the maximum brace force tested, the beam and column saw 265% and 139% more shear load than was predicted by the UFM, respectively. It is important to note that a failure may have occurred at the beam interface if sources of conservatism had not been present in the as-built specimen. It seems that typical design practices, such as using the minimum recommended fillet weld size in the AISC's *Steel Construction Manual*²⁹ and limiting the embedded bar capacity by the shear friction factor, μ , from ACI 318-19³² may permit enough robustness in the design; however, designing to

the capacity required by the UFM alone would likely not have resulted in a sufficient design.

Although the experiment described in this paper is a first step toward codifying the use of precast concrete BRBFs, a robust design methodology must be informed by more than the findings from a singular specimen. Based on the results of this research, two possibilities are proposed for future work.

First, the most promising statically determinate but unconventional connection, the lug connected only to the corbel, could be revisited. Preliminary analyses¹² showed that this connection is viable, but deeper assessment regarding strength and constructibility is needed before a connection can be designed and validated through testing. If such a connection is feasible, this would likely be the quickest and lowest-risk path to the adoption of precast concrete BRBFs into building codes because it would require less testing than the second proposed option to fully validate.

Second, a more complex testing program on precast concrete frames using steel buckling-resistanced braces could be executed to understand how forces distribute through this system and develop an entirely new design procedure. This path would have two objectives: first, to determine a methodology for distribution of forces to the precast concrete member according to member and connection stiffnesses and second, to quantify the effects of frame action on gusset plate interface force distribution in precast concrete BRBFs. If this path is taken, designs that leverage standard cross sections, member sizes, and connections could be cod-

ified. This path would likely require more experimental tests and time than development of the lug connection, but it would allow the use of common construction methods and material grades.

Acknowledgments

The authors would like to acknowledge the PCI, which provided funding for this project through a Daniel P. Jenny Fellowship, along with an advisory board. Advisory board members included Jared Brewe, Harry Gleich, Suzanne Aultman, Brandon Ross, Jon Mohle, Kim Seeber, Kevin Kirkley, and Greg Force. Tom Schaeffer, Jeff Viano, Gino Kurama, and Brandt Saxey also provided their advice and expertise. Metromont Corp. fabricated the precast concrete specimen and lent the expertise of Fanfu Fan and Corbin Martin.

References

1. Christopoulos, A. S. 2005. "Improved Seismic Performance of Buckling Restrainted Braced Frames." Master of science thesis, University of Washington, Seattle.
2. Black, C. J., N. Makris, and I. D. Aiken. 2004. "Component Testing, Seismic Evaluation and Characterization of Buckling-Restrainted Braces." *Journal of Structural Engineering* 130 (6): 880–894. [https://doi.org/10.1061/\(ASCE\)0733-9445\(2004\)130:6\(880\)](https://doi.org/10.1061/(ASCE)0733-9445(2004)130:6(880)).
3. Tremblay, R., L. Poncet, P. Bolduc, R. Neville, and R. DeVall. 2004. "Testing and Design of Buckling Restrainted Braces for Canadian Application." Presented at 13th World Conference on Earthquake Engineering, Vancouver, BC, August 1–6, 2004.
4. Newell, J., C.-M. Uang, and G. Benzoni. 2006. *Subassembly Testing of CoreBrace Buckling-Restrainted Braces (G Series): Final Report to CoreBrace, LLC*. Structural Systems Research Project Report TR-06/01. San Diego, CA: Department of Structural Engineering, University of California, San Diego.
5. AISC (American Institute of Steel Construction). 2005. *Seismic Provisions for Structural Steel Buildings*. ANSI/AISC 341-05. Chicago, IL: AISC.
6. Della Corte, G., M. D'Aniello, R. Landolfo, and F. M. Mazzolani. 2011. "Review of Steel Buckling-Restrainted Braces." *Steel Construction* 4 (2): 85–93. <https://doi.org/10.1002/stco.201110012>.
7. PCI. 2017. *PCI Design Handbook: Precast and Prestressed Concrete*. 8th ed. Chicago, IL: PCI.
8. Polat, G. 2008. "Factors Affecting the Use of Precast Concrete Systems in the United States." *Journal of Construction Engineering and Management* 134 (3): 169–178. [https://doi.org/10.1061/\(ASCE\)0733-9364\(2008\)134:3\(169\)](https://doi.org/10.1061/(ASCE)0733-9364(2008)134:3(169)).
9. Viano, J. D., and T. C. Schaeffer. 2017. "Novel Use of Buckling-Restrainted Braces in Precast Concrete Frames." *PCI Journal* 62 (5): 28–34. <https://doi.org/10.15554/pci62.5-03>.
10. Guerrero, H., T. Ji, J. Alberto Escobar, and A. Teran-Gilmore. 2018. "Effects of Buckling-Restrainted Braces on Reinforced Concrete Precast Models Subjected to Shaking Table Excitation." *Engineering Structures* 163: 294–310. <https://doi.org/10.1016/j.engstruct.2018.02.055>.
11. Oh, S., Y. C. Kurama, J. Mohle, and B. Saxey. 2021. "Seismic Design and Analysis of Precast Concrete Buckling-Restrainted Braced Frames." *PCI Journal* 66 (5): 54–83. <https://doi.org/10.15554/pci66.5-03>.
12. Kessler, H. D. 2021. "Initial Investigation of Connection Behavior for Buckling-Restrainted Braces (BRBs) in Precast Concrete Frames." Master of science thesis, Clemson University, Clemson, SC.
13. Coy, B. B. 2007. "Buckling-Restrainted Braced Frame Connection Design and Testing." Master of Science thesis. Brigham Young University, Provo, UT. <https://scholarsarchive.byu.edu/etd/992>.
14. Applied Technology Council. 2009. *Quantification of Building Seismic Performance Factors*. FEMA P695. Washington, DC: FEMA (Federal Emergency Management Agency).
15. Thornton, W. 1991. "On the Analysis and Design of Bracing Connections." In *Proceedings, National Steel Conference*. Chicago, IL: AISC. <https://www.aisc.org/globalassets/aisc/manual/15th-ed-ref-list/on-the-analysis-and-design-of-bracing-connections.pdf>.
16. AISC. *Manual of Steel Construction*. 1992. Chicago, IL: AISC.
17. Gross, J. L., and G. Cheok. 1988. *Experimental Study of Gusseted Connections for Laterally Braced Steel Buildings*. NISTIR 88-3849. Gaithersburg, MD: National Institute of Standards and Technology. <https://www.govinfo.gov/app/details/GOVPUB-C13-805dba97612cbfc1761701de8dab3446>.
18. Bjorhovde, R., and S. K. Chakrabarti. 1985. "Tests of Full-Size Gusset Plate Connections." *Journal of Structural Engineering* 111 (3): 667–684.
19. Chou, C.-C., J.-H. Liu, and D.-H. Pham. 2012. "Steel Buckling-Restrainted Braced Frames with Single and Dual Corner Gusset Connections: Seismic Tests and Analyses." *Earthquake Engineering and Structural Dynamics* 41 (7): 1137–1156. <https://doi.org/10.1002/eqe.1176>.

20. Lin, P.-C., K.-C. Tsai, A.-C. Wu, and M.-C. Chuang. 2014. "Seismic Design and Test of Gusset Connections for Buckling-Restrained Braced Frames." *Earthquake Engineering and Structural Dynamics* 43 (4): 565–587. <https://doi.org/10.1002/eqe.2360>.
21. Lin, P.-C., K.-C. Tsai, A.-C. Wu, M.-C. Chuang, C.-H. Li, and K.-J. Wang. 2015. "Seismic Design and Experiment of Single and Coupled Corner Gusset Connections in a Full-Scale Two-Story Buckling-Restrained Braced Frame." *Earthquake Engineering and Structural Dynamics* 44 (13): 2177–2198. <https://doi.org/10.1002/eqe.2577>.
22. Cui, Y., X. Xu, T. C. Becker, and W. Zhang. 2021. "Incorporating Frame Action into Seismic Design of Gusset Plates." *Journal of Structural Engineering* 147 (3). [https://doi.org/10.1061/\(ASCE\)ST.1943-541X.0002959](https://doi.org/10.1061/(ASCE)ST.1943-541X.0002959).
23. Maheri, M. R., and S. Yazdani. 2016. "Design of Steel Brace Connection to an RC Frame Using Uniform Force Method." *Journal of Constructional Steel Research* 116: 131–140. <https://doi.org/10.1016/j.jcsr.2015.09.010>.
24. Maheri, M. R., and A. Hadjipour. 2003. "Experimental Investigation and Design of Steel Brace Connection to RC Frame." *Engineering Structures* 25 (13): 1707–1714. [https://doi.org/10.1016/S0141-0296\(03\)00162-7](https://doi.org/10.1016/S0141-0296(03)00162-7).
25. Tsai, C.-Y., K.-C. Tsai, L.-W. Chen, and A.-C. Wu. 2018. "Seismic Performance Analysis of BRBs and Gussets in a Full-Scale 2-Story BRB-RCF Specimen." *Earthquake Engineering and Structural Dynamics* 47 (12): 2366–2389. <https://doi.org/10.1002/eqe.3073>.
26. Muir, L. S. 2008. "Designing Compact Gussets with the Uniform Force Method." *AISC Engineering Journal* 45 (1): 13–20.
27. AISC. 2016. *Seismic Provisions for Structural Steel Buildings*. ANSI/AISC 341-16. Chicago, IL: AISC.
28. ASCE (American Society of Civil Engineers). 2017. *Minimum Design Loads and Associated Criteria for Buildings and Other Structures*. ASCE/SEI 7-16. Reston, VA: ASCE.
29. AISC. 2017. *Steel Construction Manual*. 15th ed. Chicago, IL: AISC.
30. AISC. 2016. *Specification for Structural Steel Buildings*. ANSI/AISC 360-16. Chicago, IL: AISC.
31. Muir, L. S., and W. Thornton. 2014. *Steel Design Guide 29: Vertical Bracing Connections—Analysis and Design*. Chicago, IL: AISC.
32. ACI (American Concrete Institute). *Building Code Requirements for Structural Concrete (ACI 318-19) and Commentary (ACI 318R-19)*. Farmington Hills, MI: ACI.
33. ASTM International. 2021. *Standard Specification for High-Strength Low-Alloy Columbium-Vanadium Structural Steel*. ASTM A572/A572M-21e1. West Conshohocken, PA: ASTM International. https://doi.org/10.1520/A0572_A0572M-21E01.
34. Sutton, M. A., J. J. Orteu, H. W. Schreier, and P. Reu. 2012. "Introduction to Digital Image Correlation: Best Practices and Applications." *Experimental Techniques* 36 (1): 3–4. <https://doi.org/10.1111/j.1747-1567.2011.00798.x>.

Notation

e_b	= one-half the depth of the beam
e_c	= one-half the depth of the column
E	= elastic modulus
G	= shear modulus
H_b	= required shear force on the gusset-to-beam connection
H_c	= required axial force on the gusset-to-column connection
l_b	= length of gusset interface connected to beam
l_c	= length of gusset interface connected to column
l_g	= length of gap between bottom of beam and top of corbel
M_c	= required moment on the gusset-to-column interface
P	= required axial force
P_{beam}	= beam actuator force
P_{brace}	= brace actuator force
r	= distance between the work point and the gusset centroid
t_g	= thickness of the gusset plate
V_b	= required axial force on the gusset-to-beam connection
V_c	= required shear force on the gusset-to-column connection
α	= distance from the face of the column to the centroid of the gusset-to-column connection

- β = distance from the face of the beam to the centroid of the gusset-to-column connection
- $\Delta h_{2\%}$ = 2% story drift
- θ = angle between the centroid of the column and the centroid of the brace
- μ = shear friction factor from ACI 318
- $\sigma_b(x)$ = experimental normal stress distribution along beam-connected interface
- $\sigma_c(y)$ = experimental normal stress distribution along column-connected interface
- σ_{xx} = experimental normal stress on beam-connected interface
- σ_{yy} = experimental normal stress on column-connected interface
- $\tau_b(x)$ = experimental shear stress distribution along beam-connected interface
- $\tau_c(y)$ = experimental shear stress distribution along column-connected interface
- τ_{xy} = experimental shear stress on beam- and column-connected interfaces

About the authors



Hannah Kessler, MS, is a PCI student member and PhD student in civil engineering at Georgia Institute of Technology in Atlanta. She holds bachelor's and master's degrees in civil engineering from Clemson University in Clemson,

S.C. Her primary research interests are large- and full-scale structural testing that informs the design and codification of novel building and connection systems.



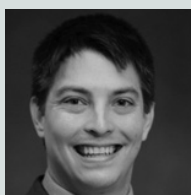
Kaitlynn Conway, PhD, completed her PhD in mechanical engineering at Clemson University and is currently in a postdoctoral position at Sandia National Laboratories in Albuquerque, N.Mex. Her primary research

interests are in solid mechanics and the fracture and failure of materials.



Laura Redmond, PhD, is a PCI member and assistant professor in the Glenn Department of Civil Engineering at Clemson University. Her research interests include advanced simulation for structural design and health

monitoring, model verification, and validation by test.



Garrett Pataky, PhD, is an assistant professor in the Department of Mechanical Engineering at Clemson University. His research interests include experimental solid mechanics to understand fracture and fatigue mechanisms of materials.

Abstract

A design method for precast concrete buckling-restrained braced frames with traditional gusset plate connections has not yet been codified. In addition, experimental data for this novel system are lacking. The primary objectives of this research were to do the following:

- Design and experimentally test a partial system under representative seismic loads.
- Determine the applicability of the uniform force method (UFM) for connection interface force distribution.

A quasi-static cyclic test was performed on a scaled, partial system. Experimental results showed that the UFM alone does not accurately predict interface forces for this system because the method does not account for frame action. Results also showed that there is some change in column base fixity as the frame undergoes larger horizontal displacements. This was the first U.S. laboratory test on a scaled, partial version of this system. Development of a codified design method would require further testing to determine an appropriate interface force distribution and quantify the change in column base fixity.

Keywords

Buckling-restrained brace, connection, uniform force method.

Review policy

This paper was reviewed in accordance with the Precast/Prestressed Concrete Institute's peer-review process. The Precast/Prestressed Concrete Institute is not responsible for statements made by authors of papers in *PCI Journal*. No payment is offered.

Publishing details

This paper appears in *PCI Journal* (ISSN 0887-9672) V. 68, No. 2, March–April 2023, and can be found at <https://doi.org/10.15554/pcij68.2-03>. *PCI Journal* is published bimonthly by the Precast/Prestressed Concrete Institute, 8770 W. Bryn Mawr Ave., Suite 1150, Chicago, IL 60631. Copyright © 2023, Precast/Prestressed Concrete Institute.

Reader comments

Please address any reader comments to *PCI Journal* editor-in-chief Tom Klemens at tklemens@pci.org or Precast/Prestressed Concrete Institute, c/o *PCI Journal*, 8770 W. Bryn Mawr Ave., Suite 1150, Chicago, IL 60631. 